Abrasive fluidized bed finishing of additive manufactured cobalt-chrome parts: effects on surface morphology and fatigue behavior

Abrasive fluidized bed finishing of additive manufactured cobalt-chrome parts: effects on surface morphology and fatigue behaviour

Eleonora Atzeni[a], Silvio Genna[b], Alessandro Salmi[a,*], Federica Trovalusci[b], Gianluca Rubino[c]

[a] Politecnico di Torino, Department of Management and Production Engineering
Corso Duca degli Abruzzi 24, 10129 Torino, Italy

[b] Università degli Studi di Roma "Tor Vergata", Department of Enterprise Engineering
Via del Politecnico 1, 00133, Roma, Italy

[c] Università della Tuscia, Department of Economics, Engineering, Society and Business Organization
Largo dell'Università, 01100, Viterbo, Italy

* Corresponding author (A. Salmi)
Email: alessandro.salmi@polito.it
Phone: (+39) 011 090.7263
Fax: (+39) 011 090.7299
ORCID: 0000-0002-7775-3014

Abstract

The possibility of processing cobalt-chrome parts by additive manufacturing opens the way to the production of complex net-shaped parts able to withstand high loads and at the same time resist to corrosive environment or thermal loads. However, the surface morphology typical of additive manufactured parts could be detrimental to the fatigue life, and finishing operations become necessary. In this paper, the adoption of abrasive fluidized bed (AFB) processing as finishing solution is explored, and the effect of the main process parameters, namely the abrasive type, treatment time and the rotational speed, on morphological features and fatigue life is investigated. Field emission gun-scanning electron microscopy and contact gauge profilometry showed an improvement in sample finishing due to the AFB process. The advantages in surface properties were related to an increase in fatigue life. The experimental results show that AFB has a beneficial effect both on finishing and fatigue behavior of additively manufactured components, a smoother surface was obtained and the crack initiation during fatigue tests was retarded.

Keywords: Additive manufacturing; Finishing; Abrasive fluidized bed; Cobalt-chrome alloys; Fatigue.

1. Introduction

Cobalt-chrome (CoCr) alloys have been gained interest in the aerospace and medical fields mainly because of their high mechanical properties combined with excellent corrosion and heat resistance [1]. The chromium content increases the corrosion resistance by generating a surface oxide layer on the part, while a higher strength is obtained by adding molybdenum (yielding stress up to 850 MPa) or nickel elements (yielding stress up to 950 MPa) in the alloy composition [2,3]. Typical applications can be found in the production of engines parts, such as engine turbines, fuel nozzles or rings, or dental/orthopaedic implants able to sustain high loads, such as dental restorations or knee implants [4,5]. Usually, CoCr parts are typically processed by casting or forging, subjected to heat treatment, and then finished by machining. When machining, the high hardness of the material, maintained at elevated temperature, results in a low machinability. In some cases, powder metallurgy has been used for the production of net-shaped parts [2].

CoCr is processable by the most common Additive Manufacturing (AM) processes for metals, that today allow a wide variety of metallic alloys to be used, including also titanium, nickel, aluminium alloys, and steels [6]. Interest in AM has been exponentially increasing, since it allows to produce fully dense parts with good mechanical performances, on the one hand, and due to the ability of AM to produce complex net-shaped parts, reducing component weight, raw material consumption, and need for additional tooling. AM starts from a three-dimensional computer-aided design (CAD) model to build up the part layer by layer, and the complexity of the model geometry is not a limit. The possibility to realize low weight parts has determined the wide application of AM in aerospace, automotive and sailing sectors, but also in the medical and dental ones, thanks to the availability of biocompatible materials.

AM techniques for metal parts production include Powder Bed Processes (PBF), both with a laser or electron beam energy source, and Directed Energy Deposition (DED). The feedstock in metal AM is typically in form of spherical powder particles, with a diameter variable from 20 μm to 150 μm, depending on the specific process, that is smaller powder is used in laser powder bed fusion (L-PBF) and coarser powder in electron beam powder bed fusion (EB-PBF) and DED [7]. In general, alloys used in the additive techniques show a better resistance and lower ductility than the corresponding ones made with conventional techniques [8]. However, significant differences in the material structure, quality, and performance can be found by performing the different AM processes [9]. In the case of CoCr alloys, the high strength combined with good ductility can be attributed to the steady-state hardening and to the induced hardening rate during the melting process of the layers [10]. In particular, the alloy will have microstructural variations caused by the melting and cooling phases of the layers, which act as an aging process that allows the structure to pass from the metastable phase γ-fcc to the stable phase ε-hcp [11]. However, one of the limitations lies in the mechanical anisotropy during the manufacturing process, which in some cases affects the final performance [12]. It will also present problems related to fatigue, while the failure mechanism will depend on different co-factors, such as surface finish or defects present in the part, which will be

related to the type of layered micro- and macro-structure [13]. For example, the EB-PBF process is performed in a vacuum with powder pre-heating; conversely, L-PBF uses an inert gas with only platform heating, and different results in terms of microstructure and residual stresses are found. Additionally, a Hot Isostatic Pressing (HIP) treatment is commonly adopted after EB-PBF production to close internal porosities, determining a beneficial effect on fatigue endurance.

The relation between the fatigue properties and the surface morphology is well established; an increase in the roughness can be detrimental to the fatigue life [14]. L-PBF parts exhibit a finer surface than EB-LBF, and DED parts are the roughest, but all of them should be finished if parts undergo fatigue loads. In addition, the high surface roughness of additively manufactured parts might not comply with stringent requirements of some mechanical applications. Elaborated external and internal surfaces may not be easily accessible for finishing and their original topography could not be adequately improved. The resulting relatively poor fatigue strength is AM technology's most significant acceptability challenge when considered for the production of net-shape parts for fatigue applications [15].

Since the finishing quality of additive metal parts is still an issue, the present study investigates the feasibility of using an Abrasive Fluidized Bed (AFB) to improve the surface finish and, at the same time, the fatigue behaviour of CoCr parts produced by L-PBF. In a previous work, this technology was found to be effective on titanium alloys [16]. AFB is a promising technology based on loose abrasives taken in a fluid state [17]. The fluidized abrasives can surround the component as a liquid medium, making AFB suitable for the complex geometries typical of AM [18]. AFB finishing can be considered more effective than other technologies based on abrasives because of the higher impact speeds between the abrasives and substrates, achievable by moving the workpiece inside the fluidization chamber [19]. The main drawbacks in finishing by AFB are: (i) the prediction of the finishing quality and (ii) the limited productivity; these issues are even more evident in the case of complex geometries and when finishing uniformity and geometrical accuracy are required. Cheng et al. [20] proposed a multiscale multiphysics simulation-based approach to model and simulate the AFB machining against the component shape and dimensional accuracy control. They found that the media consistently create the largest difference in the machining system. The multiscale multiphysics modelling and simulation was also adopted by Shao et al. [21] to optimize the AFB machining to improve the process quality, costs and delivering time, in the field of aerofoil structures and their typical complex profiles. To the author’s knowledge, there are no studies in the literature about the AFB finishing of CoCr parts produced by L-PBF, and on the resulting fatigue properties

In the present study, axial-symmetric CoCr samples were fabricated by L-PBF. They were rotated at high speed inside a fluidized bed and subjected to the impact of abrasive media. Two steel abrasive types, cut wire pellet and angular grit, were compared to find the most effective one. The fatigue failure of treated and untreated samples was determined by rotating bending tests. The effect of AFB process parameters on morphological features and fatigue life was investigated.

2. Materials and methods

In this section the geometry of the samples used in the experimental activity, the fabrication step and the AFB experimental setup are detailed. Moreover, the methodology used for the assessment of the surface morphology and fatigue behaviour is explained.

2.1. Sample design

The sample was designed according to the ISO 1143:2010 standard [22], with axial-symmetric shape and a test zone 12 mm long and 6 mm in diameter. An additional cylindrical extension at one side of the sample, 12 mm in diameter and 70 mm in length, was added to clamp the sample during the AFB process (red part in Figure 1). This extension was cut off after the finishing treatment. Such design was adopted to systematically investigate the influence of AFB treatments on the fatigue life of samples.

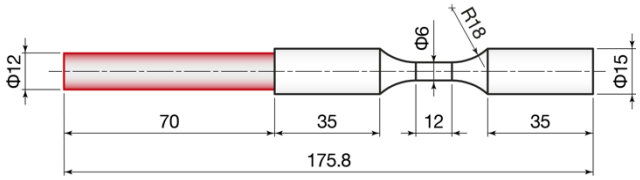

Figure 1 – Geometry of the test sample (all dimensions in mm).

2.2. Sample fabrication

Twenty-seven test samples were built by the L-PBF system EOS M 400-4, using EOS CobaltChrome MP1 powder, both by EOS GmbH (Krailling, Germany). The EOS CobaltChrome MP1 powder is developed for high-temperature engineering applications and medical implants [23]. The properties of EOS CobaltChrome MP1 laser processed parts fulfil the ISO 5832-4 and ASTM F75 standards of cast CoCrMo implant alloys [24,25].

Table 1. Nominal chemical composition [26]

Weight percentage					
Co	Cr	Mo	Si	Mn	others
60-65	26-30	5-7	<1	<1	<1

Table 2. Physical and mechanical properties of EOS CobaltChrome MP1 parts, stress relieved, 6 hours at 1150 °C under inert argon atmosphere [26]

Property	Value
Density (kg/dm^3)	8.3
Modulus of elasticity (GPa)*	200 ± 20
Yield strength (Rp 0.2%) (MPa)*	600 ± 50
Tensile strength (MPa)*	1100 ± 100
Elongation at break (%)*	min 20

* Tensile testing according to ISO 6892-1:2009 (B) Annex D, proportional test pieces, diameter of the neck area 5 mm, original gauge length 25 mm

Table 1 lists the nominal chemical composition and Table 2 summarizes the main physical and mechanical properties attested by the supplier. The average particle size of EOS CobaltChrome MP1 is 80 µm, and standard process parameters for were used to fabricate the samples.

2.3. Abrasive Fluidized Bed finishing

The AFB equipment used in the finishing treatment is reported in Figure 2: the sample is clamped on a horizontal shaft and rotated at a constant speed; the abrasive media is fluidized in a vertical column (100 mm in diameter and 500 mm high) by a porous plate distributor, supplying a fluidizing gas (compressed air). The sample rotation ensures the process uniformity on the whole surface of the sample.

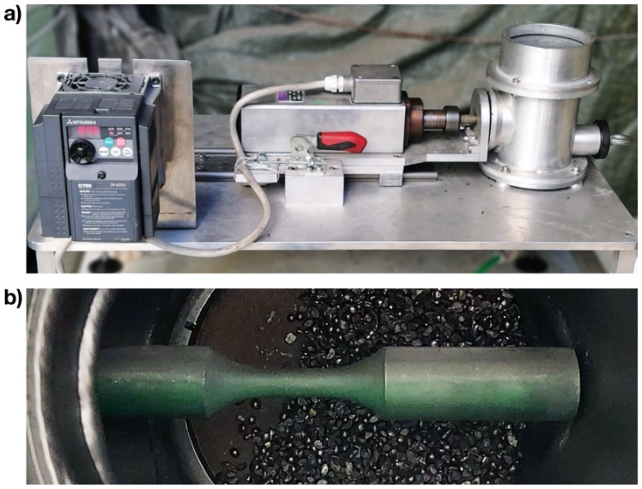

Figure 2. (a) AFB equipment and (b) a sample in the abrasive fluidized bed (AFB)

During the tests, the effect of the media and of the rotating speed were studied. Thus, two different media (Figure 3) and two levels of rotational speed were adopted:

- cut wire steel pellet (HRC 45-55, 1 mm rod-shaped);
- angular steel grit (HRC 64, mesh size 12 µm);
- low speed (3000 rpm);
- high speed (4800 rpm).

The abrasive particles and the fluidizing gas were both inert, and no reactions occurred in the column. Samples were exposed to the repeated impacts by the abrasive for different treatment times (2, 4, 6, and 8 hours). Specifically, at the end of each treatment time, the treated sample was removed from the AFB system, inspected, and held again in the system for continuing the finishing treatment. Treatment times higher than 8 hours were not considered because of the limited industrial interest in longer processes. For each set of working conditions, three repetitions of the test were performed. In total, 12 samples were used to test the finishing conditions.

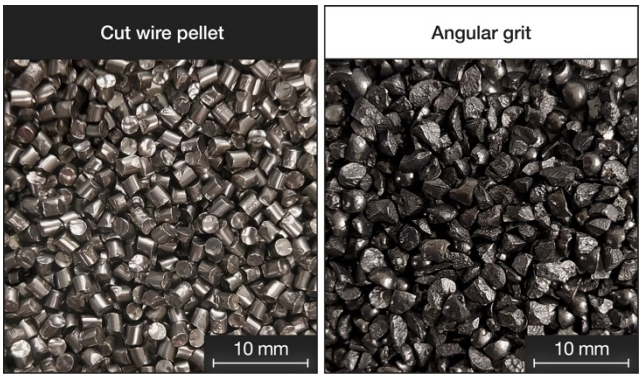

Figure 3. Steel abrasives tested: cut wire pellet and angular grit

2.4. Surface characterization

The influence of the operational parameters, namely, abrasive type, treatment time, and rotational speed, on the finishing performance was evaluated. The interaction between the abrasive particle and the substrates was analysed in terms of morphological features, inspecting surfaces by using a Leo Supra 35 Field Emission Gun – Scanning Electron Microscopy (FEG-SEM) by Zeiss (Thornwood, NY, USA) by a Talysurf CLI 200 contact gauge profilometer by Taylor Hobson (Leicester, United Kingdom). Profiles along the longitudinal direction were measured on each sample to analyse the morphology after finishing. Each profile had a length of 12 mm, acquired by setting the spacing to 1 µm, and the measurement speed to 1 mm/s. Three-dimensional maps, 3 × 4 mm^2, were also acquired, with spacing 2 µm and a measurement speed of 1 mm/s. All the roughness parameters were evaluated according to ISO 21920-2:2021 standard [27]. Moreover, the actual diameter of the samples and their weight were measured before and after treatment to have an indication of the material loss caused by the finishing process.

2.5. Fatigue characterization

Preliminary, the fatigue failure of the as-built specimen and that of the AFB treated (8h) specimens, for each finishing condition, was determined by rotating bending tests performed on a A 2TM831 rotating bending machine by Italsigma (Forlì, Italy). Once fixed the load (17.5 kg), the number of cycles to failure was determined for each specimen. All specimens were rotated at the same speed of 150 rpm. This low speed was set during the rotating bending test to avoid the occurrence of dynamic loads generated by the imperfect symmetry of the samples, typical of components obtained by additive processes. The condition beneficial to the fatigue life was thus identified. Further fatigue tests were performed for this condition and as-built samples, and the load was varied to build the Wohler curves. A total of 15 samples were used to characterize the fatigue behaviour.

3. Results and discussion

In Figure 4, the surface topography before and after treatment in the fluidized bed is shown. From the image, three-dimensional maps show how the media treat the surfaces: the as-built surface is

characterized by sharp picks, due to the presence of semi-molten powder agglomerates. On the contrary, the treated samples show a smoother surface. In general, a smoother surface was achieved by increasing treatment time and rotational speed; however, from Figure 4, the mechanism that allows the finishing is not visible. Thus, SEM analysis was conducted with the aim of understanding better the effect of the media and of the speed.

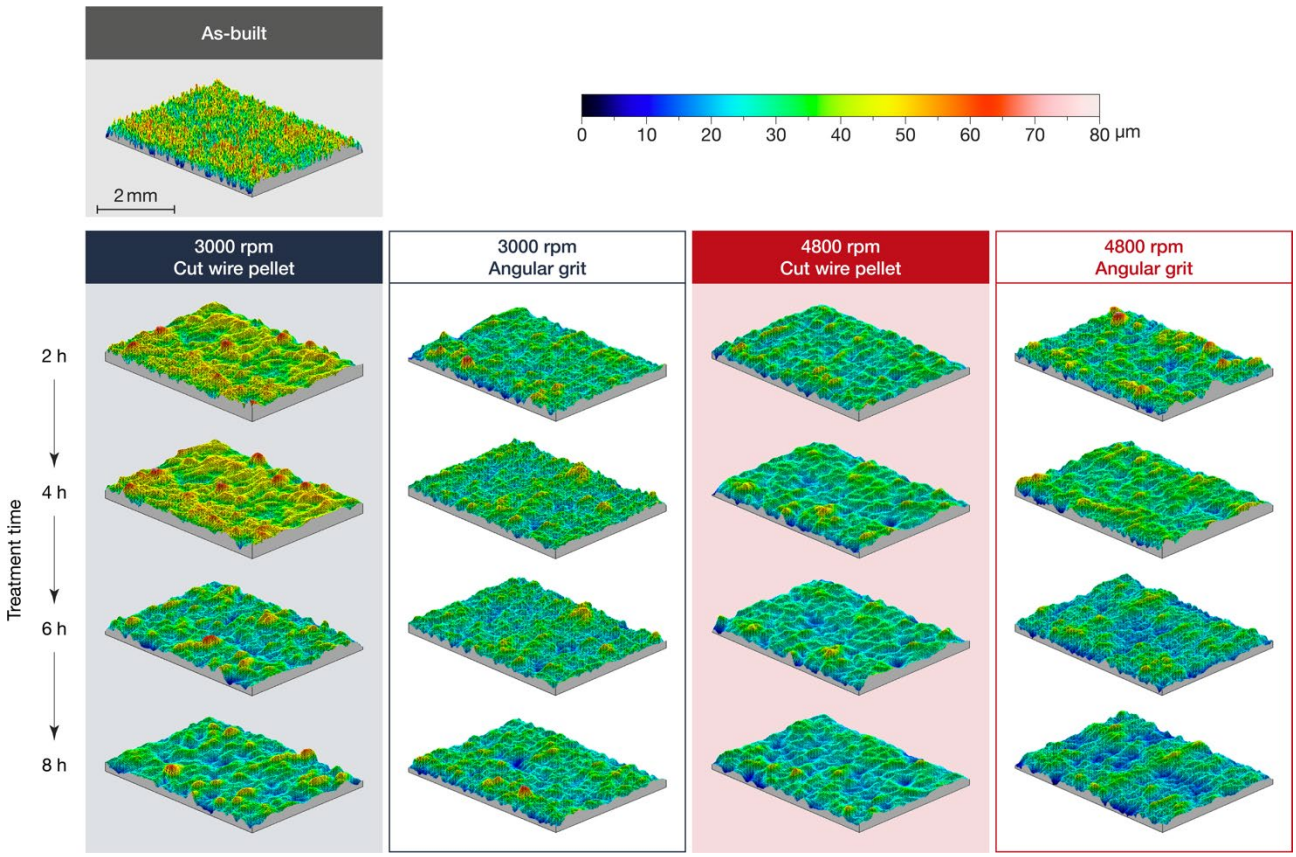

Figure 4. Topographical three-dimensional maps of an as-built sample and sample treated in the AFB with different process parameters

In Figure 5, SEM images of the as-built and treated samples are reported after 8 hours for both the abrasive type and rotational speed: the difference between the topography of the as-built sample and the one obtained after the AFB process is clearly visible. The treated surface quality highly depended on the abrasive type, and rotational speed. The as-built surface is characterized by a high density of peaks and valleys that are very close to one other, also due to the presence of only partially sintered powder particles. Considering low magnification (first row), the AFB treatment was effective in removing semi-molten powder agglomerates; the aspect of the as-built surface was significantly modified after the AFB treatment, and the starting agglomerates were utterly flattened. Considering higher magnification (lower row), the differences between the media and the speeds appear clearer: the morphology of the surface obtained by cut wire appears different from the one obtained by angular grit; the first appears affected by plastic deformation of the peaks; the media

act like "small-hammers" that crush the roughness; this is more visible at low speed (3000 rpm). On the contrary, the angular grit acts like a "cutting tool" that takes away the roughness; the effect is visible at high speed (4800 rpm), where the surface appears smoother, and some pores emerge. The pores are typical of the additive manufactured parts and are generally visible when sectioning is done. This confirms that the angular grit determined micro-cutting mechanism, while cut wire established the ploughing mechanism.

The different mechanism of the two media can be ascribed either to the geometry (flat or angular) or to the difference in terms of size. In particular, the cut wire particle is larger than angular grit, for this reason it is able to perform a more effective action at lower rotational speed. By comparing the behaviour of the two abrasives at low rotational speed, the cut wire had greater energy in the impact and higher effect on finishing since the particle mass is greater. The effect of the sample speed becomes more significant than the effect of the abrasive speeds when a fast rotation is imposed, as in the considered working conditions.

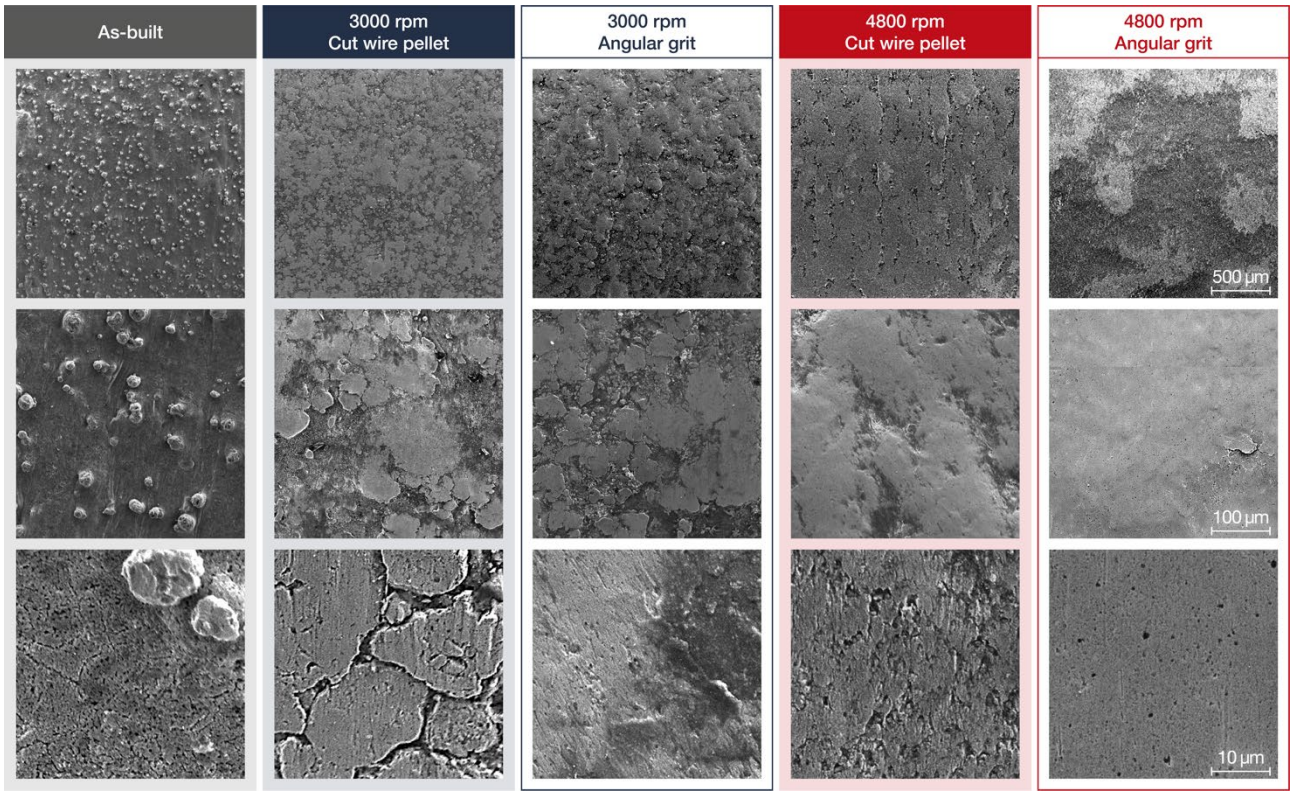

Figure 5. Morphology of an as-built sample and samples treated for 8 hours in the AFB varying abrasive type and rotational speed

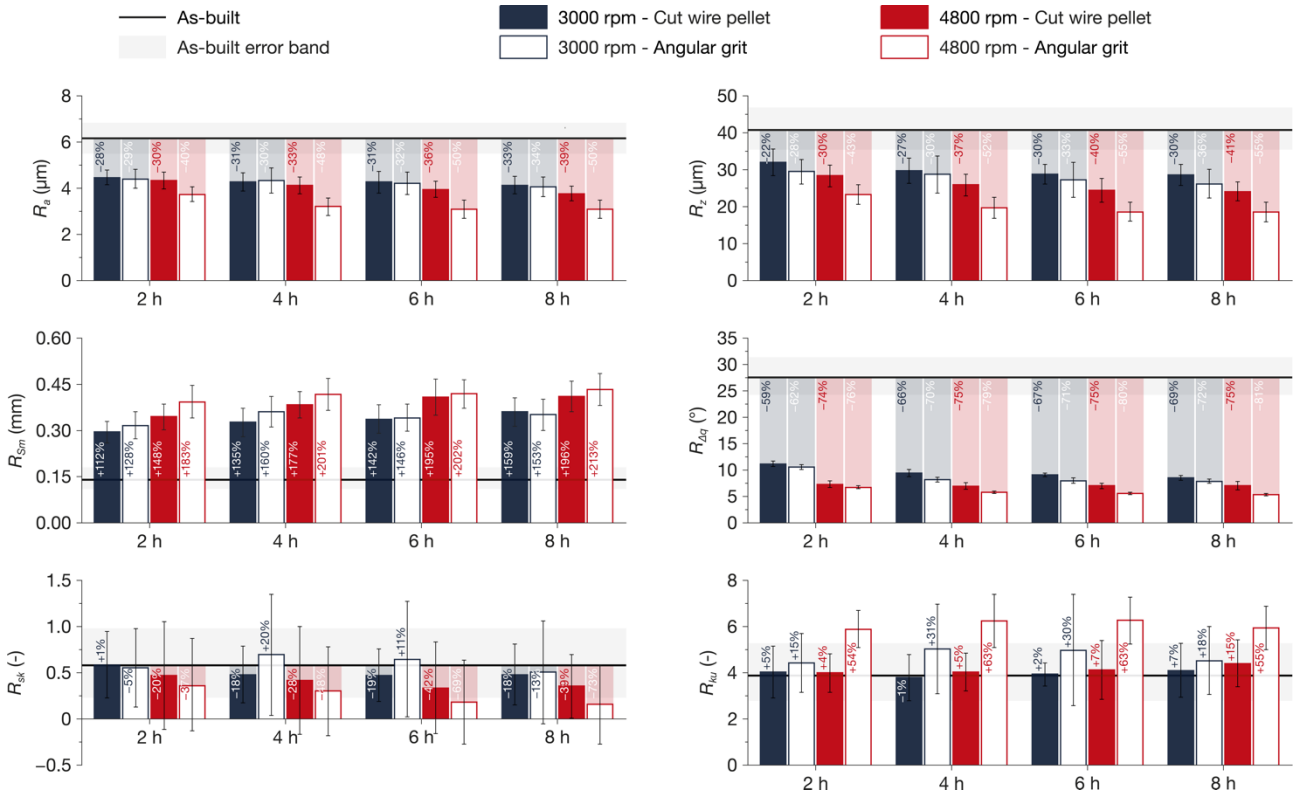

Figure 6. Normalized roughness parameters of samples treated in the AFB with different process parameters

To better analyse the morphology improvement led by the AFB process, the time evolution of roughness parameters versus AFB process conditions is displayed in Figure 6 for the two abrasive types. Due to the variability of the L-PBF process, the as-built properties slightly differ on the samples. Thus, for each roughness parameter, the average value of the as-built parts ($\bar{R}_{as-built}$) is represented in the Figure 6, with the error band. Moreover, for each parameter and treatment, the values of roughness parameters are also reported in terms of average values ($\bar{R}_{treated}$) and standard deviations; to put in evidence the percentage variation ($\Delta\bar{R}_{\%}$) from the average value of the as-built samples the following equation is used:

$$\Delta\bar{R}_{\%} = \frac{\bar{R}_{treated} - \bar{R}_{as-built}}{\bar{R}_{as-built}} \cdot 100 \quad (1)$$

Regarding the effect of the rotational speed, lower values of roughness parameters were always obtained when high-speed impacts between particles and surface took place. Higher treatment times allowed roughness improvement, however higher removal was obtained in the first 2 hours of treatment, then asymptotic trend was established for all conditions. This observation confirms that treatment times longer than 8 hours are not of interest. A significant variation of roughness parameters (–40% Ra and –43% Rz) was observed using angular grit at higher rotational speed (4800 rpm) after 2 hours of treatment, confirming that this abrasive was most effective than cut wire, as suggested by Figure 5.

The variation of sample dimension in Table 3 and Figure 7(a), and of sample weight in Table 4 and Figure 7(b), confirm the progressive material loss. It is worth to note that the variation of diameter was

evaluated in the section where break occurred, whereas the variation of weight also considered the areas not affected by the break. To compare results, normalized values were used. Thus, for each *j* treatment, the diameter of the treated sample ($d_{j,treated}$) was referred to the original as-built diameter of the same sample ($d_{j,as-built}$), and the percentage deviation($\Delta d_{j\%}$) was also expressed by using Eq. (2). Analogously, the weight ($w_{j,treated}$) was normalized and the percentage deviation ($\Delta w_{j\%}$) was expressed by using Eq. (3).

$$\Delta d_{j\%} = \frac{d_{j,treated} - d_{j,as-built}}{d_{j,as-built}} \cdot 100 \quad (2)$$

$$\Delta w_{j\%} = \frac{w_{j,treated} - w_{j,as-built}}{w_{j,as-built}} \cdot 100 \quad (3)$$

Regardless of the used abrasive type, a higher reduction of diameter and weight were found for the higher rotational speed (in red colour in Figure 7). Maximum reductions (-0.13%) were found for angular grit (empty bars). This confirms what observed with the SEM analysis: this medium allows the cutting mechanism; while the cut wire the plastic deformation. With increasing the treatment time, a strain hardening effect was induced on the impacted surface making more difficult further material removal. As a matter of fact, the values of diameter and weight after 6 hours of treatment are quite stable, confirming that the process is less effective at longer treatment times. Only for the cut wire abrasive (solid bars) after 6 hours a further variation was observable, probably due to micro fatigue phenomenon during AFB treatment.

Table 3. Sample dimension before and after the AFB finishing treatment with different process parameters

Diameter (mm)	**3000 rpm**		**4800 rpm**	
Treatment time	**Cut wire pellet**	**Angular grit**	**Cut wire pellet**	**Angular grit**
As-built	6.01	5.97	6,01	6.04
2 h	5.99	5.90	5.88	5.90
4 h	5.98	5.88	5.81	5.83
6 h	5.98	5.87	5.78	5.78
8 h	5.97	5.86	5.75	5.77

Table 4. Sample weight before and after the AFB finishing treatment with different process parameters

Weight (g)	**3000 rpm**		**4800 rpm**	
Treatment time	**Cut wire pellet**	**Angular grit**	**Cut wire pellet**	**Angular grit**
As-built	188.87	188.51	188.90	188.96
2 h	188.79	188.40	188.75	188.78
4 h	188.76	188.35	188.70	188.74
6 h	188.73	188.33	188.69	188.72
8 h	188.69	188.31	188.67	188.71

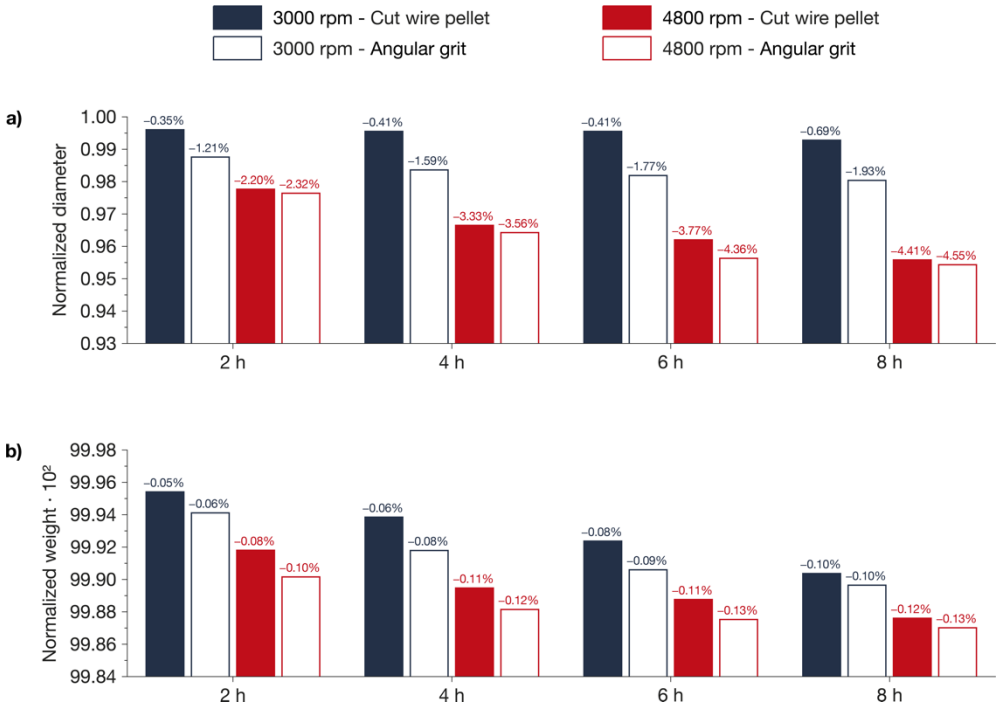

Figure 7. Variation of (a) dimensions and (b) weight
of samples treated in the AFB with different process parameters

The number of cycles to failure under fatigue tests is reported in Figure 8, both for as-built samples and samples treated for 8h. For both the considered abrasive types, AFB treatment was beneficial to increasing the fatigue life when the higher rotational speed was used. The angular grit was confirmed to be the most effective abrasive, which determined the more significant improvement.

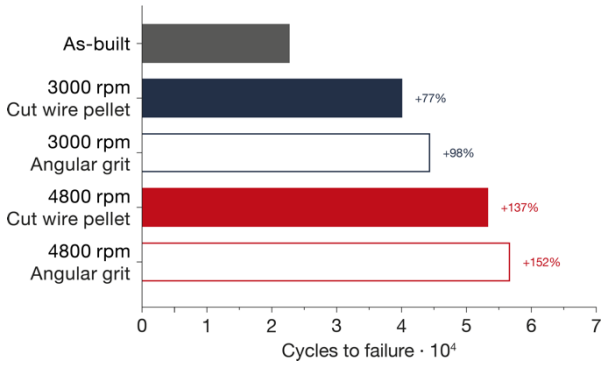

Figure 8. Number of cycles to failure for a fixed load (17.5 kg) of samples
before and after the AFB finishing treatment with different process parameters

The different effect on fatigue found for the two abrasive types can be related to different micro fatigue phenomenon determined by AFB treatment. It is worth noting that the Co-Cr specimens are characterized by a fine grain microstructure and very high hardness, thus the during the finishing, the action of the cut wire abrasive allows the peaks on the external layer to be flatted by ploughing mechanism but does not affect the inner layer nor generates a significant compressive stress that leads to improvement on fatigue life. This is confirmed by Figure 8: angular media provide the best fatigue life, where lower compressive stresses are present due to the shape and lower mass of the abrasives.

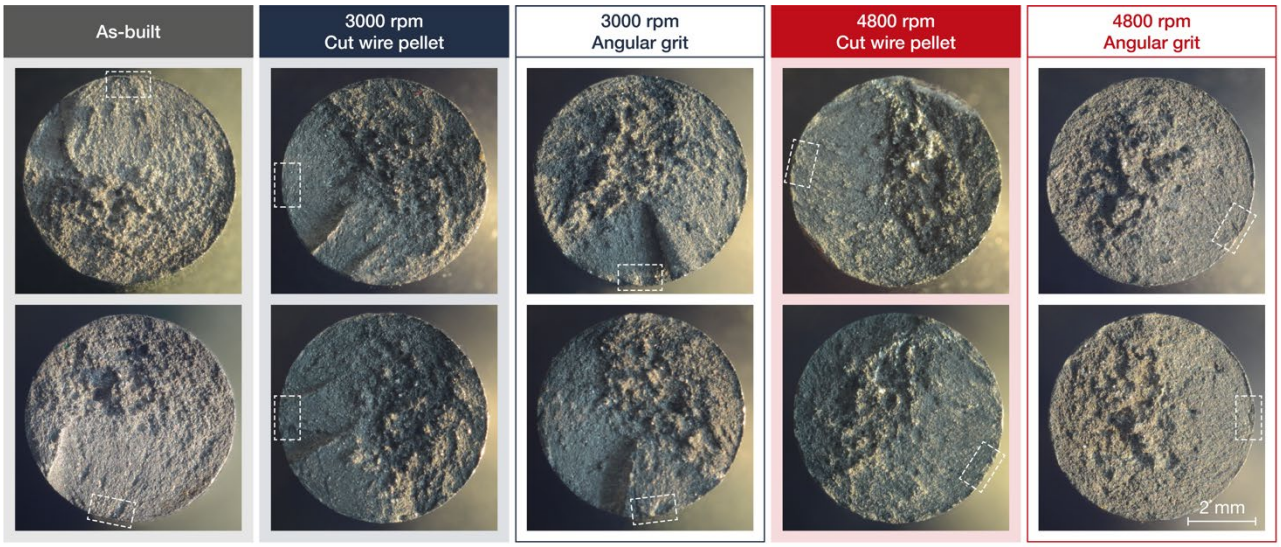

Figure 9. Fracture surfaces with fatigue crack initiation sites highlighted (dashed rectangle) after fatigue tests of an as-built sample and samples treated for 8 hours in the AFB varying abrasive type and rotational speed

In Figure 9 the fracture surfaces after fatigue tests are shown. By analysing the images, almost the same extension of crash break area (rough zone) was observed for different treatment conditions. However, when angular media is adopted, the crash break area is observed in the centre of the section; while the opposite occurs in the case on the as-built sample and when cut wire media is adopted (i.e. the crash break area is on a side); this suggests that the finishing of the external surface was so effective that the cracks started from internal defects.

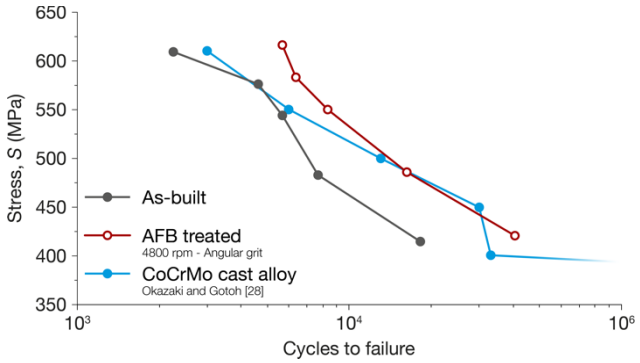

Figure 10. Wohler curve for as-built, AFB treated sample (angular grit, 4800 rpm for 8 h) and CoCrMo cast alloy samples from the literature [28].

The most beneficial condition in terms of fatigue life (angular grit, 4800 rpm, 8 h) was further investigated; thus, more samples were treated, fatigue tests were performed by varying the applied load, the S-N curves of AFB treated, and as-built samples were calculated. In Figure 10, the Wohler curves for the as-built and AFB samples are reported. As expected, the curve of the AFB samples is shifted upward/rightward referred to the as-built one. This is due to the higher surface finishing obtained by the treatment. Moreover, on the same figure the curve of CoCrMo cast alloy finished

by 600 grit sandpaper, as described in Okazaki and Gotoh [28], is included for comparison. Besides the as built surface is quite rougher than the cast part, at high loads the fatigue life is analogous. For lower loads, the finishing treatment becomes mandatory in additive manufactured parts and AFB treated parts show a similar or even higher fatigue behaviour than finished cast parts of analogous material. In fact, by removing surface asperities, the internal defects (pores/inclusions) act as crack initiation origin and the porosity in L-PBF parts is typically lower that cast parts [29]. As further improvement, an HIPping treatment may be considered on Co-Cr parts since it determines the pores closure in AM components [30].

4. Conclusions

Finishing of CoCr samples fabricated by L-PBF was performed by treatment inside an AFB. Two abrasive media were used, and for both the AFB process was found to be effective in improving the finishing and the fatigue behaviour of samples. The morphology of surfaces obtained by AM was wholly modified by the high-speed impact between media and surface; semi-molten powder agglomerates, typical of AM, were removed. In this work, the AFB process was applied to axial-symmetric samples for fatigue characterization, but the process is suitable for the complex geometries obtained by AM.

Experimental results showed that abrasive type, treatment time, and rotational speed in AFB were influential on the finishing and fatigue life of samples. Smoother morphologies were found by increasing treatment time and rotational speed when angular steel grit is used as abrasive media.

Rotating bending tests were performed, and a higher number of cycles to failure was obtained when the rotational speed inside AFB was set at the higher value, 4800 rpm. The Wohler curve of treated samples was translated to larger values of the number of cycles since the smoother and defective-free surface of AFB treated surfaces retarded the crack initiation during fatigue tests.

Other processes, i.e., laser and shot peening, could improve metal surfaces roughness and fatigue limits. In a previous work by the authors [16] AFB was compared to laser in terms of effects on roughness and fatigue life improvement. Both the processes were found to be effective on titanium alloys. However, compared to other processes, AFB has many advantages. For example, laser main drawbacks are related to safety and costs, shot peening is a high-pressure process with drawbacks related to safety, control, running costs, and environmental impact. Contrarily, AFB treatment is performed at low pressure, can be easily controlled, does not require specific caution for safety and environmental impact, can be scaled and completely automated without expensive procedures [17]. Relevant is the fact that the FB process is suitable for complex geometry, typical of AM [18], improving at the same time finishing and fatigue behaviour. When the AFB process is optimized, the crack initiation during fatigue tests is retarded, being the treated surface smoother and defective-free.

Acknowledgements

The authors would like to gratefully acknowledge the support and generosity of the Interdepartmental Centre for Integrated Additive Manufacturing (IAM@PoliTo) at the Politecnico di Torino, Torino, Italy, and the Turin Additive Lab (TAL), Torino, Italy, for the resources to perform the research activities.

Declarations

Authors' contributions: E. Atzeni: investigation, writing - original draft and review, resources; A. Salmi: visualization, investigation, resources, writing - review & editing; S. Genna: investigation, writing - original draft; F. Trovalusci: investigation, formal analysis, writing - original draft; G. Rubino: methodology, investigation, formal analysis, writing - original draft.

Funding: This research was partially supported by the Interdepartmental Center for Integrated Additive Manufacturing IAM@PoliTo at the Politecnico di Torino, Torino, Italy.

Availability of data and materials: The manuscript has no associated data. Data will be made available upon request.

Compliance with ethical standards

Competing interests: The authors declare that they have no known competing financial interests or personal relationships that could have influenced the work reported in this paper.

Ethical approval: Not applicable.

Consent to participate: Not applicable.

Consent to publish: Not applicable.

References

1. Hong JH, Yeoh FY (2020) Mechanical properties and corrosion resistance of cobalt-chrome alloy fabricated using additive manufacturing. Materials Today: Proceedings 29:196-201. doi:10.1016/j.matpr.2020.05.543

2. Zaman HA, Sharif S, Kim D-W, Idris MH, Suhaimi MA, Tumurkhuyag Z (2017) Machinability of Cobalt-based and Cobalt Chromium Molybdenum Alloys - A Review. Procedia Manufacturing 11:563-570. doi:10.1016/j.promfg.2017.07.150

3. Sahoo P, Das SK, Paulo Davim J (2019) Tribology of materials for biomedical applications. In: Mechanical Behaviour of Biomaterials. pp 1-45. doi:10.1016/b978-0-08-102174-3.00001-2

4. Padrós R, Punset M, Molmeneu M, Velasco AB, Herrero-Climent M, Rupérez E, Gil FJ (2020) Mechanical Properties of CoCr Dental-Prosthesis Restorations Made by Three Manufacturing Processes. Influence of the Microstructure and Topography. Metals 10 (6). doi:10.3390/met10060788

5. Gibon E, Amanatullah DF, Loi F, Pajarinen J, Nabeshima A, Yao Z, Hamadouche M, Goodman SB (2017) The biological response to orthopaedic implants for joint replacement: Part I: Metals. Journal of Biomedical Materials Research Part B: Applied Biomaterials 105 (7):2162-2173. doi:10.1002/jbm.b.33734

6. Mirzaali MJ, Bobbert FSL, Li Y, Zadpoor AA (2019) Additive Manufacturing of Metals Using Powder Bed-Based Technologies. In: Additive Manufacturing. pp 93-145. doi:10.1201/9780429466236-4

7. Mergulhão MV, Das Neves MDM (2018) Characteristics of Biometallic Alloy to Additive Manufacturing Using Selective Laser Melting Technology. Journal of Biomaterials and Nanobiotechnology 09 (01):89-99. doi:10.4236/jbnb.2018.91008

8. Aversa A, Marchese G, Bassini E (2021) Directed Energy Deposition of AISI 316L Stainless Steel Powder: Effect of Process Parameters. Metals 11 (6). doi:10.3390/met11060932

9. Lewandowski JJ, Seifi M (2016) Metal Additive Manufacturing: A Review of Mechanical Properties. Annual Review of Materials Research 46 (1):151-186. doi:10.1146/annurev-matsci-070115-032024

10. Wang Z, Tang SY, Scudino S, Ivanov YP, Qu RT, Wang D, Yang C, Zhang WW, Greer AL, Eckert J, Prashanth KG (2021) Additive manufacturing of a martensitic Co–Cr–Mo alloy: Towards circumventing the strength–ductility trade-off. Additive Manufacturing 37:101725. doi:https://doi.org/10.1016/j.addma.2020.101725

11. Yufan Zhao YK, Kenta Aoyagi, Kenta Yamanaka, Akihiko Chiba (2020) Isothermal γ → ε phase transformation behavior in a Co-Cr-Mo alloy depending on thermal history during electron beam powder-bed additive manufacturing. J Mater Sci Technol 50 (0):162-170. doi:10.1016/j.jmst.2019.11.040

12. Hitzler L, Alifui-Segbaya F, Williams P, Heine B, Heitzmann M, Hall W, Merkel M, Öchsner A (2018) Additive Manufacturing of Cobalt-Based Dental Alloys: Analysis of Microstructure and

Physicomechanical Properties. Advances in Materials Science and Engineering 2018:8213023. doi:10.1155/2018/8213023

13. Dikova T (2018) Bending fracture of Co-Cr dental bridges, produced by additive technologies: experimental investigation. Procedia Structural Integrity 13:461-468. doi:https://doi.org/10.1016/j.prostr.2018.12.077

14. Bagehorn S, Wehr J, Maier HJ (2017) Application of mechanical surface finishing processes for roughness reduction and fatigue improvement of additively manufactured Ti-6Al-4V parts. International Journal of Fatigue 102:135-142. doi:https://doi.org/10.1016/j.ijfatigue.2017.05.008

15. Mower TM, Long MJ (2016) Mechanical behavior of additive manufactured, powder-bed laser-fused materials. Materials Science and Engineering: A 651:198-213. doi:https://doi.org/10.1016/j.msea.2015.10.068

16. Atzeni E, Genna S, Menna E, Rubino G, Salmi A, Trovalusci F (2021) Surface Finishing of Additive Manufactured Ti-6Al-4V Alloy: A Comparison between Abrasive Fluidized Bed and Laser Finishing. Materials 14 (18):5366

17. Barletta M (2009) Progress in abrasive fluidized bed machining. Journal of Materials Processing Technology 209 (20):6087-6102. doi:https://doi.org/10.1016/j.jmatprotec.2009.04.009

18. Atzeni E, Barletta M, Calignano F, Iuliano L, Rubino G, Tagliaferri V (2016) Abrasive Fluidized Bed (AFB) finishing of AlSi10Mg substrates manufactured by Direct Metal Laser Sintering (DMLS). Additive Manufacturing 10:15-23. doi:https://doi.org/10.1016/j.addma.2016.01.005

19. Ribezzo A, Calignano F, Salmi A, Atzeni E, Pietrobono F, Trovalusci F, Rubino G Finishing of metal additive manufactured parts by abrasive fluidized bed machining. In: Riemer O, Savio E, Billington D, Leach RK, Phillips D (eds) 18th International Conference of the European Society for Precision Engineering and Nanotechnology, EUSPEN 2018, 2018. euspen, pp 271-272

20. Cheng K, Shao Y, Bodenhorst R, Jadva M (2017) Modeling and Simulation of Material Removal Rates and Profile Accuracy Control in Abrasive Flow Machining of the Integrally Bladed Rotor Blade and Experimental Perspectives. Journal of Manufacturing Science and Engineering 139 (12). doi:10.1115/1.4038027

21. Shao Y, Adetoro OB, Cheng K (2020) Development of multiscale multiphysics-based modelling and simulations with the application to precision machining of aerofoil structures. Engineering Computations 38 (3):1330-1349. doi:10.1108/ec-10-2019-0473

22. ISO (2010) ISO 1143:2010, Metallic materials — Rotating bar bending fatigue testing

23. Bassoli E, Denti L (2018) Assay of Secondary Anisotropy in Additively Manufactured Alloys for Dental Applications. Materials 11 (10). doi:10.3390/ma11101831

24. ISO (2014) ISO 5832-4:2014, Implants for surgery — Metallic materials — Part 4: Cobalt-chromium-molybdenum casting alloy. Genève

25. ASTM International (2018) ASTM F75-12, Standard Specification for Cobalt-28 Chromium-6 Molybdenum Alloy Castings and Casting Alloy for Surgical Implants (UNS R30075). ASTM F75-12. ASTM International, West Conshohocken (USA)

26. EOS GmbH (2022) Material Data Sheet EOS CobaltChrome MP1. http://www.e-manufacturing.it/downloads/EOS_CobaltChrome_MP1.pdf. Accessed 7-July-2022

27. ISO (2021) ISO 21920-2:2021, Geometrical product specifications (GPS) — Surface texture: Profile — Part 2: Terms, definitions and surface texture parameters. Genève

28. Okazaki Y, Gotoh E (2002) Corrosion Fatigue Properties of Metallic Biomaterials in Eagle’s Medium. Materials Transactions 43 (12):2949-2955. doi:10.2320/matertrans.43.2949

29. Schweiger J, Güth J-F, Erdelt K-J, Edelhoff D, Schubert O (2020) Internal porosities, retentive force, and survival of cobalt–chromium alloy clasps fabricated by selective laser-sintering. Journal of Prosthodontic Research 64 (2):210-216. doi:10.1016/j.jpor.2019.07.006

30. du Plessis A, Macdonald E (2020) Hot isostatic pressing in metal additive manufacturing: X-ray tomography reveals details of pore closure. Additive Manufacturing 34. doi:10.1016/j.addma.2020.101191